Boundary-Layer Meteorology (2024) 190:47
https://doi.org/10.1007/s10546-024-00885-7

RESEARCH ARTICLE

Revisiting a Drag Partition Model For Canopy-Like Roughness Elements

Elia Buono[1] · Gabriel G. Katul[2] · Davide Vettori[1] · Davide Poggi[1] · Costantino Manes[1]

Received: 11 April 2024 / Accepted: 9 September 2024 / Published online: 22 October 2024

Abstract
Turbulent flows over a large surface area (S) covered by n obstacles experience an overall drag due to the presence of the ground and the protruding obstacles into the flow. The drag partition between the roughness obstacles and the ground is analyzed using an analytical model proposed by Raupach (Boundary-Layer Meteorol 60:375-395, 1992) and is hereafter referred to as R92. The R92 is based on the premise that the wake behind an isolated roughness element can be described by a shelter area A and a shelter volume V. The individual sizes of A and V without any interference from other obstacles can be determined from scaling analysis for the spread of wakes. To upscale from an individual roughness element to n/S elements where wakes may interact, R92 adopted a background stress re-normalizing instead of reducing A or V with each element addition. This work demonstrates that R92's approach results in a linear background stress reduction in A and V only when the ratio of n/S is small, due to a low probability of wake interactions. This probabilistic nature suggests that up-scaling from individual to multiple roughness elements can be re-formulated using stochastic averaging methods proposed here. The two approaches are shown to recover R92 under plausible conditions. An alternative scaling for the shelter volume is also proposed here using thermodynamic arguments of work and dissipation though the final outcome remains similar to R92. Comparisons between R92 and available data spanning more than two decades after R92 on blocks and vegetation-like roughness elements confirm the practical utility of R92. The agreement between R92 and this updated databases of experiments and simulations confirm the potential use of R92 in large-scale models provided that the relevant parameters accommodate certain features of the roughness element type (cube versus vegetation-like) and, to a lesser extent, their configuration throughout S. Last, a comparison between R92 and models based on first-order closure principles with constant mixing length suggests that R92 can outperform such models when evaluated across a wide range of roughness densities.

Keywords Canopy turbulence · Drag partition · Sheltering · Superposition · Wakes

✉ Elia Buono
elia.buono@polito.it

[1] Dipartimento di Ingegneria dell'Ambiente, del Territorio e delle Infrastrutture, Politecnico di Torino, Torino, Italia

[2] Department of Civil and Environmental Engineering, Duke University, Durham, North Carolina, USA

1 Introduction

The separate treatment of drag exercised by canopy-like roughness elements and the underlying surface is now needed in a plethora of science and engineering applications. These applications span hydrodynamic behavior and sediment transport within vegetated channels (Huai et al. 2021; Vargas-Luna et al. 2015; Nepf 1999, 2012; Aberle and Järvelä 2013), flow above urban areas (Grimmond and Oke 1999; Martilli et al. 2002; Giridharan and Emmanuel 2018; Ng et al. 2011; Ishugah et al. 2014; Ren et al. 2018; Jamei et al. 2020; Coceal and Belcher 2004), wind related erosion of surfaces covered by roughness elements (Kok et al. 2012; Shao 2008; Raupach et al. 1993; Ravi et al. 2010; Chappell et al. 2019; Okin et al. 2006; Okin 2008), soil-derived dust injection into the atmosphere (Marticorena and Bergametti 1995; Zender et al. 2003; Shao and Dong 2006; Yu and Ginoux 2022), deposition of aerosol particles onto vegetation and forest floor (Katul et al. 2010, 2011), coastal dune dynamics (Hesp 2002), wind related tree damage (Gardiner et al. 2000; Gardiner 2021), to name a few. In the early 1990s, an under-appreciated analytical approach was put forth for such drag partition over surfaces exhibiting canopy-like geometries (Raupach 1992). This approach, labeled hereafter as R92, was derived for a deep turbulent boundary layer using scaling analysis and physical constraints on the spread of wakes behind isolated obstacles (Marticorena and Bergametti 1995; Shao and Yang 2008). In R92, the total turbulent shear stress τ with an associated friction velocity u_* over a rough surface of a given roughness geometry is the sum of the shear stress on all roughness elements (τ_R) and the ground stress on the underlying surface (τ_S). That is, the force balance per unit ground area leads to:

$$\tau = \rho u_*^2 = \tau_R + \tau_S, \tag{1}$$

where ρ is the fluid density. In the absence of vegetation or obstacles protruding into the flow, $\tau = \rho u_*^2 = \tau_S$. The presence of roughness elements reduce the ground stress in their wake so that $\tau_S/\tau < 1$. This wake effect is associated with a reduced mean velocity or, equivalently, a stress deficit behind the roughness element. In the stress deficit representation, an effective shelter area can be defined as the area where the ground shear stress is set to be zero so as to obtain an equivalent stress deficit distributed over the entire ground area S. From this definition, the shelter area for a single obstacle can be defined as (Raupach 1992):

$$A = \iint \left(1 - \frac{\tau_S\,(x,\,y)}{\tau_{S0}}\right) dxdy, \tag{2}$$

where $\tau_S(x,\,y)$ is the actual ground stress at any point $(x,\,y)$ on S and τ_{S0} is the presumed undisturbed stress, set to be equal to the actual ground stress far away from any roughness element. Using similar arguments, an effective shelter volume can also be defined as (Raupach 1992):

$$V = \iiint \left(1 - \frac{\phi\,(x,\,y,\,z)}{\phi_0}\right) dxdydz, \tag{3}$$

where $\phi = \rho\alpha C_E\,(U)\,U^2$ is the local drag per unit volume on a sparse array of identical roughness elements with the local drag coefficient C_E and frontal area per unit volume α. As before, subscript 0 refers to the undisturbed state or background state far away from any roughness element. In some studies, it was also interpreted as the stress value in the absence of roughness elements (Shao and Yang 2008), though the interpretation of R92 is preferred here.

To proceed from these definitions to drag partition between the ground and the obstacles, R92 employed two plausible hypotheses. The first hypothesis is a scaling analysis that deals with the nature of the effective shelter area and shelter volume to yield:

$$A = c_A bh \frac{U_h}{u_*}, \tag{4}$$

and:

$$V = c_V bh^2 \frac{U_h}{u_*}, \tag{5}$$

where b and h are the width and height of the isolated roughness element, U_h is the mean flow velocity at $z/h = 1$ as schematized in Fig. 1, c_A and c_V are unknown scaling coefficients that vary with the aspect ratio b/h. In R92, $c_A \sim c_V \sim 1$ when $h >> b$ and $c_A \sim c_V \sim b/h$ when $h << b$. A plausible expression that allows a gradual transition between these two end-member limits may be written as $c_A \sim c_V \sim (\sqrt{h^2 + b^2})/h$. In support of the first hypothesis, R92 argued that the shelter area (or volume) is dictated by how vorticity spawned by the roughness element advects and diffuses out downwind from the obstacle location. R92 conjectured that the vorticity produced at the obstacle advects at a velocity that scales with U_h and spreads away from the longitudinal axis at a velocity that scales with u_*. The first hypothesis is grounded in 'text-book' scaling arguments regarding how wakes spread in boundary free flows (Tennekes and Lumley 1972), where U_h is analogous to the so-called irrotational free stream velocity outside the wake. The second hypothesis is that the combined effect of randomly distributed roughness elements on a surface can be obtained by random superposition of individual shelter area or volume. The essence of this approximation is rather subtle as already pointed out in prior studies (Shao and Yang 2008) and unpacking it partly motivated the present work. In R92, the background (or far field) stress is defined as τ_{S0} in the absence of any obstacles ($i = 0$). Adding a single obstacle ($i = 1$) at a random location generates a shelter area A and an associated τ_{S1} that reduces τ_{S0} by a factor $(1 - A/S)$. Proceeding to $i = 2$ (i.e. adding another obstacle), R92 argued that the background state to use now should be τ_{S1} (already reduced from τ_{S0}). This τ_{S1} is, once again, presumed to be uniformly distributed over the same ground area S. Adding another obstacle ($i = 3$) at a random location reduces the background state, now set to τ_{S2}, by another $1 - (A/S)$, and so forth. Since A/S is small at each random superimposition associated with a sequential increase in i or roughness element addition, the background stress state at $i - 1$ can be reduced and then uniformly re-distributed over the entire area S. Using these two hypotheses, the ground stress τ_{Sn} and drag force per unit area τ_{Rn} for a set of n identical roughness elements randomly superimposed on S are given by:

$$\tau_{Sn} = \tau_{S0} \left(1 - \frac{A}{S}\right)^n, \tag{6}$$

and:

$$\tau_{Rn} = \frac{n\Phi}{S} \left(1 - \frac{V}{Sh}\right)^n, \tag{7}$$

where S is presumed to be sufficiently large compared to A, A is unaltered by successive additions of roughness elements (or increase in i), $\Phi = \rho C_R(U_h) bh U_h^2$ is the drag force on an isolated roughness element, with U_h being the mean velocity at the canopy top, and $C_R(U_h)$ is the drag coefficient for an isolated roughness element. The global drag coefficient C_R can be related to the local drag coefficient C_E using:

$$C_R = \frac{1}{hU_h^2} \int_0^h C_E(U) U^2 dz. \tag{8}$$

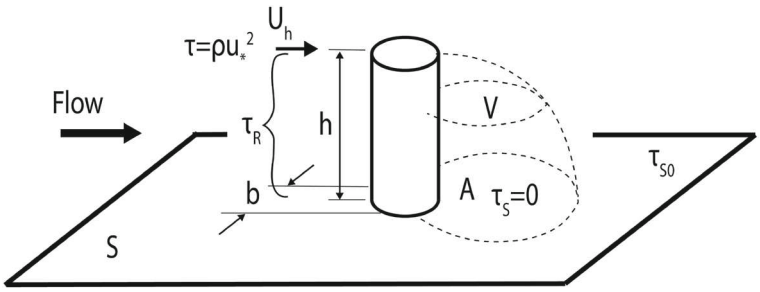

Fig. 1 Schematic view of the main variables assuming the canopy is a rod characterized by a height h and a width b. The flow is from left to right. U_h and u_* are both defined at the canopy top. The background state is characterized by a ground stress that would have existed in the absence of an obstacle (i.e. τ_{S0})

The ambiguity in R92 about the effect of roughness changes on the definition of U_h was already raised in a prior study (Shao and Yang 2008). This ambiguity will also be considered here and shown to be less of an issue as R92 predicts U_h/u_* not U_h.

The goal of this contribution is to answer two inter-related questions: (i) to what extent can the equations in Raupach (1992) be derived while relaxing or further clarifying some of the approximations linked to the underlying hypotheses? (ii) to what degree can the model in Raupach (1992), or a revised version of it (as proposed here), reproduce the wealth of new data sets that include simulations and experiments over different canopy-like roughness values accrued over the last 3 decades? Thus, a practical outcome of this investigation is an 'upgrade' of model parameters that can be readily employed in conjunction with R92 for differing roughness types.

2 Appraisal of R92

The appraisal begins by revising the original analysis of R92 from a discrete to a continuous case so as to accommodate the proper statistical averaging in the background stress states. The combination of canopy stress and ground stress is then invoked to obtain the drag partition.

2.1 Shelter volume analysis

While plausible, Eqs. 6 and 7 are derived using simplified scaling of vorticity diffusion and advection. An alternative approach assumes that the turbulent kinetic energy (TKE) dissipation rate (ϵ) scales as:

$$\epsilon \sim \frac{TKE}{\tau_d}, \tag{9}$$

where TKE scales as u_*^2, u_* is the friction velocity and τ_d is a relaxation time describing the time it takes to dissipate the most energetic eddy. The problem then is reduced to choices for τ_d. Given a certain roughness density, the main constraint on τ_d is eddy penetration into the array of roughness elements (i.e. a roughness sublayer already exists with such a roughness density). In this case, τ_d is proportional to l_I/u_*, where l_I is a characteristic scale which tends to either h or b based on the aspect ratio b/h ($l_I \sim h$ if $b/h \to 0$ and $l_I \sim b$ if $b/h \to \infty$). Analogously, ϵ can be also defined as the energy injected per unit time (and unit mass of fluid) by the work of the drag against the mean flow. The work per unit mass is, by definition,

force times distance per mass. This work per unit mass is assumed to be entirely converted to heat through ϵ within a τ_d period. Now, setting the force to Φ, the distance to $U_h\tau_d$, and the mass to ρV leads to:

$$\epsilon \sim \frac{u_*^2}{\tau_d} \sim \frac{\Phi U_h}{\rho V} = \frac{\rho C_R\,(U_h)\,bhU_h^2 U_h}{\rho V} = \frac{C_R bhU_h^3}{V}, \tag{10}$$

where V is the shelter volume, i.e. the volume of fluid contained in the near field of the wake generated by each roughness element, Φ is the drag on the individual element, C_R is the drag coefficient. From Eq. 10, V for an array of roughness elements scales as:

$$V = C_V C_R bh\frac{U_h^3}{u_*^2}\tau_d, \tag{11}$$

where C_V is a scaling parameter. For an array of tall roughness elements, the argument in R92 can be reduced to selecting a τ_d that scales with h/u_*. For blunt roughness elements, τ_d may scale as b/u_* or $\sqrt{bh}/u_*$. Similarly, the shelter area A can be found as:

$$A = C_A V/h = C_A C_V C_R b\frac{U_h^3}{u_*^2}\tau_d, \tag{12}$$

where C_A is a scaling parameter that depends on the roughness density and shape. Since $C_R \sim u_*^2/U_h^2$, the R92 results are recovered when selecting a τ_d that scales as h/u_*. To emphasize the role of τ_d, they are repeated here as:

$$V = C_V bh\frac{U_h}{(u_*/h)}, \tag{13}$$

and:

$$A = C_A C_V b\frac{U_h}{(u_*/h)}. \tag{14}$$

2.2 Ground stress analysis

The dynamically interesting features in R92 are first highlighted by contrasting them to a more intuitive starting point. Suppose the analysis commences using a finite but very large surface area S characterized by an undisturbed ground shear τ_{S0}. As before, placing a single roughness element on S leads to a single shelter area and a reduction to the overall ground shear stress by $\tau_{S0}A/S$ based on the definition of A. That is, for the $i = 1$ roughness element configuration, what is outside the shelter area A is assumed to be not affected by the presence of the roughness element or shelter area. This assumption means that τ_{S0} outside A is the same as the background or undisturbed value whereas $\tau_S = 0$ inside A as before. When τ_S remains undisturbed outside the wake, a further addition of a roughness element randomly placed on S will lead to an equal $\tau_{S0}A/S$ stress deficit, unless the second element is placed inside the wake area of the first. However, this situation may be deemed unlikely (i.e. in a probabilistic manner) when $A/S << 1$. Extending this argument without modification to the placement of the nth element now leads to a ground shear stress given by:

$$\tau_{Sn} = \tau_{So}\left(1 - \frac{nA}{S}\right). \tag{15}$$

This 'additive' approach appears plausible provided that $nA/S << 1$ and wakes have very low probability of interacting with each other because of the random placement. Although

such approach should be compatible with very low roughness density, it fails with the increasing of n. This result is consistent with Eq. 6 when noting that the two leading order terms in the expansion of $(1+\epsilon_o)^n$ (i.e. R92) are $1+n\epsilon_o$ (i.e. linear additions of A/S) for $\epsilon_o = A/S << 1$. This difference between Eq. 15 and R92 implies that the normalization and re-distribution of the background ground shear stress state is introducing non-linearities that cannot be captured by area superposition alone. The new physics in R92 (i.e. the background stress normalization) circumvents the naive assumption that new elements will always fall outside the existing wake areas irrespective of the number of elements already present on S. In fact, re-normalizing the background stress for each addition of an element accounts for the fact that with increasing n, the probability of placing an element within nA can no longer be ignored. While R92 addressed this issue intuitively, it is argued in the present work that the proper random placement of roughness elements requires a stochastic averaging approach to ground stress determination even though A is assumed constant for each additional element. Thus, placing a roughness element must be evaluated using its expected effect on the shear stress, which is labeled as $E(\tau_S)A$, where $E(\tau_S)$ is the expected value of τ_S when choosing a random point on S already covered with $n-1$ roughness elements. For a general ground shear stress condition $\tau_S(x, y)$, $E(\tau_S)$ can be estimated from:

$$E(\tau_S) = \lim_{k\to\infty}\left(\frac{1}{k}\sum_{i=1}^{k}\tau_S(x_i, y_i)\right). \tag{16}$$

This expression is the sample mean of τ_{Si} as $k \to \infty$ points are randomly chosen over S. The formulation in Eq. 16 is equivalent to the integral mean of $\tau_S(x, y)$ over the surface S because:

$$E(\tau_S) = \frac{1}{S}\int_S \tau_S dA. \tag{17}$$

The ground stress for a series of n roughness elements successively and randomly placed on surface S can now be obtained. First, Eq. 2 can be generalized by defining $\tau_{S,i}$ as the resulting ground shear stress after the ith element is randomly placed on S and $\tau_{S,i-1}$ as the stress condition before placement of the ith element. Hence,

$$A_i = \int_S\left(1 - \frac{\tau_{S,i}}{\tau_{S,i-1}}\right)dA. \tag{18}$$

Multiplying Eq. 18 by the expected value of the undisturbed ground shear state at $i-1$ results in:

$$E\left(\tau_{S,i-1}\right)A_i = E\left(\tau_{S,i-1}\right)S - \int_S \frac{E\left(\tau_{S,i-1}\right)}{\tau_{S,i-1}}\tau_{S,i}dA. \tag{19}$$

To recover the formulation in R92, it is necessary to assume that $E\left(\tau_{S,i-1}\right)/\tau_{S,i-1} \sim 1$ and this assumption must be satisfied for all subsequent ground shear stress fields $\tau_{S,i}$. Under this assumption,

$$E\left(\tau_{S,i}\right) = E\left(\tau_{S,i-1}\right)\left(1 - \frac{A_i}{S}\right). \tag{20}$$

One can trace the chain of successive products all the way back to the undisturbed condition τ_{S0}. For simplicity, this undisturbed state τ_{S0} must be assumed to be $E(\tau_{S0})$. For this approximation,

$$\tau_{Sn} = \tau_{S0}\prod_{i=1}^{n}\left(1 - \frac{A_i}{S}\right). \tag{21}$$

Once again, if A_i/S is a constant set to A/S, R92 is recovered. The outcome in Eq. 21 highlights another intrinsic assumption in R92, A_i/S is independent of i. Note that the probabilistic interpretation herein proposed highlights and clarifies that R92 is expected to perform reasonably when the variations of ground shear stress do not deviate much from their expected value (i.e. $E\left(\tau_{S,i-1}\right)/\tau_{S,i-1} \sim 1$). This expectation is deemed reasonable when roughness elements are distributed uniformly without forming evident gaps or clusters. Moreover, as already anticipated, A_i/S can be considered independent of i only for relatively sparse roughness configurations, meaning R92 is expected to fail for high values of roughness densities.

2.3 Drag analysis

A similar approach can be used to arrive at a definition of the drag acting on the roughness elements. That is,

$$E(\Phi) = \lim_{k\to\infty}\left(\frac{1}{k}\sum_{i=1}^{k}\rho C_R\left(U_h\left(x_i, y_i\right)\right) bhU_h^2\left(x_i, y_i\right)\right). \tag{22}$$

As before, the drag is distributed over an equivalent ground area S. The U_h is assumed to be in equilibrium with the roughness elements placed over S so that:

$$E(\Phi) = \frac{1}{S}\int_S \rho C_R\left(U_h\right)(bh)U_h^2 dxdy. \tag{23}$$

To arrive at the depth-integrated value over h, Φ is defined using a local drag coefficient C_E that varies with the local mean velocity U as:

$$\Phi = \rho C_R bhU_h^2 = \int_0^h \rho C_E(U)\, bU^2 dz. \tag{24}$$

Putting together Eqs. 23 and 24, a definition of $E(\Phi)$ as an integral of a discrete drag per unit volume can be derived and is given by:

$$E(\Phi) = \frac{1}{S}\int_S\left[\frac{1}{h}\int_0^h \rho(bh)C_E(U)\, U^2 dz\right]dxdy. \tag{25}$$

Analogous to the ground shear stress used to evaluate the drag by random superposition of n roughness elements onto S, a general form of effective shelter volume V_i of the ith roughness element added onto a configuration of $i-1$ roughness elements characterized by a $U_{i-1}(x, y, z)$ can be defined as:

$$V_i = \int_{Sh}\left[1 - \frac{C_E\left(U_i\right)U_i^2}{C_E\left(U_{i-1}\right)U_{i-1}^2}\right]dV. \tag{26}$$

Multiplying Eq. 26 by the expected value of the drag on the $i-1$ element, a relation similar to Eq. 19 that highlights the implicit hypothesis of random super-imposition for drag contributions emerges and is given by:

$$E\left(\Phi_{i-1}\right)V_i = E\left(\Phi_{i-1}\right)Sh - \int_{Sh}\rho bh\frac{E\left(C_E\left(U_{i-1}\right)U_{i-1}^2\right)}{C_E\left(U_{i-1}\right)U_{i-1}^2}C_E\left(U_i\right)U_i^2 dV. \tag{27}$$

The hypothesis that:

$$\frac{E\left[C_E(U)U^2\right]}{C_E(U)U^2} \approx 1, \tag{28}$$

is needed to recover the formulation for the drag on the ith roughness element randomly superimposed on a $i-1$ existing elements. This formulation is given by:

$$E\left(\Phi_i\right) = E\left(\Phi_{i-1}\right)\left(1 - \frac{V_i}{Sh}\right). \tag{29}$$

It is assumed that the hydrodynamic behavior of a given random configuration of roughness elements is independent of the order in which these elements have been placed. If so, the expected drag on the ith element corresponds to the expected value of all other $i-1$ elements previously arranged when the ith element is added. Consequently, the total drag at the n element configuration is given by:

$$F_R = \sum_{1}^{n} E(\Phi_i) = nE(\Phi_n), \tag{30}$$

and:

$$F_R = n\Phi_0 \prod_{i=1}^{n}\left(1 - \frac{V_i}{Sh}\right). \tag{31}$$

The R92 is recovered from Eq. 31 when $V_i/(Sh) = V/(Sh)$ is presumed constant. In other words, as in Eq. 21, an intrinsic assumption in R92 is that $V_i/(Sh)$ is independent of i.

Analogously to the ground stress analysis, R92 is expected to perform reasonably for uniformly distributed (i.e. $E\left[C_E(U)U^2\right]/C_E(U)U^2 \approx 1$) and relatively sparse roughness elements (i.e. $V_i/(Sh)$ is independent of i).

2.4 Total shear stress

To obtain τ_{Sn} and τ_{Rn} for n roughness elements as defined by R92, the effective shelter area and volume of each element subsequently added onto S must be considered constant and equal to A and V. This hypothesis is valid only when roughness elements are sparse and wakes of each element are similar in size to those of an isolated roughness element. When adding sequentially a single element to n elements onto S, the overall frontal area index $\lambda = nbh/S$ increases because n increases and S is constant. When a certain value of the frontal area index is achieved, R92 suggests to allow n and S to tend to infinity by maintaining a constant λ. This assumption leads to:

$$\tau_{Sn} = \tau_{S0}\left(1 - \frac{\lambda A}{nbh}\right)^n, \tag{32}$$

and:

$$\tau_{Rn} = \lambda\frac{\Phi_0}{bh}\left(1 - \frac{\lambda V}{nbh^2}\right)^n. \tag{33}$$

As $n \to \infty$ and $S \to \infty$, this formulation tends to:

$$\tau_S = \tau_{S0}\exp\left(-\frac{\lambda A}{bh}\right), \tag{34}$$

and:

$$\tau_R = \lambda \frac{\Phi_0}{bh} \exp\left(-\frac{\lambda A}{bh}\right). \tag{35}$$

Here, the identity:

$$\lim_{n\to+\infty} \left(1 + \frac{x}{n}\right)^n = \exp(x), \tag{36}$$

was employed. Recalling that drag acting on the isolated element is $\Phi_0 = \rho C_R (bh) U_h^2$ and the undisturbed ground shear stress can be generically expressed as $\tau_{So} = \rho C_S U_h^2$ and putting all these together yields:

$$\tau = \rho C_S U_h^2 \exp\left(-\frac{\lambda A}{bh}\right) + \rho \lambda C_R U_h^2 \exp\left(-\frac{\lambda V}{bh^2}\right). \tag{37}$$

Upon setting $V = Ah$ and $A_f = bh$, Eq. 37 simplifies to:

$$\frac{1}{\gamma^2} = (C_S + \lambda C_R) \exp\left(-\lambda \frac{A}{A_f}\right), \tag{38}$$

where $\gamma = U_h/u_*$. Equation 38 remains valid irrespective of the precise definition of shelter area. From Eq. 4, $A/A_f = c_A(U_h/u_*)$ is constant and Eq. 38 can be formulated as:

$$\frac{1}{\gamma^2} = (C_S + \lambda C_R) \exp(-c_A \lambda \gamma). \tag{39}$$

Eq. 39 can be expressed as:

$$Y \exp(-Y) = B_o;\ Y = \frac{c_A \lambda \gamma}{2};\ B_o = \frac{1}{\sqrt{C_s + \lambda C_R}} \frac{c_A \lambda \gamma}{2}. \tag{40}$$

The solution to this algebraic equation (i.e. $Y = f(B_o)$) can be expressed in terms of the Lamberts W function. However, the Lamberts W function (or its related function - the product logarithm) cannot be expressed in terms of elementary functions and numerical methods must be employed to solve this equation. Few properties of this equation have already been highlighted by R92 and are briefly repeated: no solutions for $B_o > \exp(-1)$ exist, a single solution for $B_o = \exp(-1)$ (i.e. $Y = 1$) exist, and two solutions for $B_o < \exp(-1)$ also exist. The two solutions are $Y_1 < 1$ and $Y_2 > 1$. The physically realistic solution is the $Y_1 < 1$.

The drag partition problem is now reduced to inferring C_S and C_R (as well as c_A) from measured γ and λ. This inference is conducted using nonlinear optimization - matching Eq. 39 to measured γ and λ while setting C_S, C_R, and c_A to constants whose values are optimized from least-squares analysis.

2.5 A simplified expression for drag partition

Before proceeding to the experimental evaluation, a number of comments can be made about a popular variant of R92. From definitions and provided that $A/S = V/(Sh)$ remains constant, a simpler version of R92 discussed in other studies (Raupach et al. 1993; Shao and Yang 2008) can be directly recovered. Equations 6 and 7 can be expressed as:

$$\tau_{Sn} = \rho C_S U_h^2 \left(1 - \frac{A}{S}\right)^n;\ \tau_{Rn} = \rho C_R \lambda U_h^2 \left(1 - \frac{A}{S}\right)^n = (\beta\lambda)\tau_{Sn}, \tag{41}$$

where $\beta = C_R/C_S$. It directly follows that the drag partition problem of τ into its two components for n elements reduces to:

$$\frac{\tau_{Sn}}{\tau} = \frac{1}{1+\beta\lambda}; \quad \frac{\tau_{Rn}}{\tau} = \frac{(\beta\lambda)}{1+\beta\lambda}. \tag{42}$$

This equation has the desirable features that for large $\beta\lambda$, $(\tau_{Sn}/\tau) \to 0$ and $\tau_{Rn}/\tau \to 1$ consistent with logical expectations that the total drag is carried by drag on the n elements and not by the ground. Conversely, when $\beta\lambda \to 0$, $(\tau_{Sn}/\tau) \to 1$ and $\tau_{Rn}/\tau \to 0$, again as expected. The expressions in equation 42 can be stated as:

$$\gamma^2 = \frac{1}{1+\beta\lambda}\frac{1}{C_S}\left(1-\frac{A}{S}\right)^{-n}. \tag{43}$$

For nA/S being small,

$$\frac{1}{\gamma^2} = (1+\beta\lambda)C_S\left(1-n\frac{A}{S}\right) = (C_S + C_R\lambda)\left(1 - c_A\lambda\gamma\right). \tag{44}$$

That is, Eq. 39 becomes reasonably approximated by its linear form in Eq. 44 for small nA/S. This simplified version illustrates the quadratic dependence of γ^{-2} on λ.

3 Experimental evaluation

Data presented in R92 along with recent experiments are here combined to evaluate R92 across different roughness types (see details in Table 1). The data sets refer to the most studied obstructions: prismatic objects referred to as "cubes" (Walter et al. 2012; Macdonald et al. 1998; Yang et al. 2016; Macdonald 2000) and plant-shaped objects referred to as "plants", both artificial (Raupach 1992; Walter et al. 2012; Poggi et al. 2004; Kang et al. 2019) and real (Wolfe and Nickling 1996; Lancaster and Baas 1998), and from laboratory and field experiments as well as numerical simulations (Yang et al. 2016). The data sets cover the following ranges of λ: from 3×10^{-4} to 5 for real plants, from 3.7×10^{-3} to 0.2 for artificial plants and from 3.9×10^{-3} to 9.1×10^{-2} for cubes.

In the majority of the experiments, λ and γ were measured and combined with Eq. 39 to obtain the unknowns C_R and c_A by means of non-linear least squares regression. Experimental γ values were computed from direct measurements of mean flow velocity at the canopy top when available or computed trough the log-law of the wall (Wolfe and Nickling 1996; Lancaster and Baas 1998; Yang et al. 2016; Macdonald et al. 1998). The third degree of freedom (i.e. C_S) in Eq. 39 was fixed at values provided in each study to ensure robust regression fits. When a value of C_S was not provided, we arbitrarily set $C_S = 2 \times 10^{-3}$ for laboratory experiments and $C_S = 4 \times 10^{-3}$ for field experiments. The nonlinear regression analysis was conducted using MATLAB's (Mathworks, Natick, Massachusetts, USA) built in function "lsqnonlin". The optimized values of C_R and c_A are summarized in Table 2 and Fig. 2. The optimized curve for each dataset is presented in Fig. 3, while the modelled u_*/U_h, calculated using optimized parameters from Table 2, are compared with the experimental values from the literature in Fig. 4.

The effectiveness of R92 is evaluated using the coefficient of determination R^2, which is reported in Table 2 for all data sets employed. Equation 39 provides a good ($R^2 > 0.9$) description of u_*/U_h across most data sets. Consistent with model assumptions, Eq. 39 appears less effective for high values of λ. To test the limits of the model, R^2 were also computed for three different ranges of λ: 0−0.03, 0.03−0.3 and above 0.3. The resulting R^2

Table 1 Summary of collected experimental and simulation results from the literature (* field experiment, ** numerical simulation). Here, the Data ID is used as legend in Figs. 3, 4, 5, 6, 8. The h is the roughness element height, b is the roughness element average breadth $b = A_f/h$, A_f is the roughness element frontal area, λ is the frontal area index, γ is the ratio U_h/u_* (supplied in each work) and C_S is the ground surface drag coefficient ($'$ is used when not provided by the authors)

Reference	Data ID	Type	h [mm]	b [mm]	$\lambda \times 10^{-3}$	γ	$C_S \times 10^3$
Raupach (1992)	RTE	Plant	6	6	10.8–182	12.5–5.4	3.0
	OL	Cube	4.7	4.8	3.9–15.6	15.411.2	3.0
	GJR*	Plant	–	–	253–5000	3.9–2.6	3.0
Walter et al. (2012)	WA_pla	Plant	100	40	15–202	14.6–6.6	1.8
	WA_cub	Cube	80	40	16.7–173	11.8–5.0	1.9
Macdonald (2000)	MCD_al	Cube	100	100	50–330	6.9–3.9	2.0′
	MCD_st	Cube	100	100	50–330	5.6–2.8	2.0′
Wolfe and Nickling (1996)*	WLF	Plant	820–1200	1100–1320	0.3–232	13.5–6.2	5.2
Lancaster and Baas (1998)*	LAN	Plant	90–110	90–110	39–212	11.8–5.8	4.0′
Yang et al. (2016)**	YAN_al	Cube	25	25	30–250	8.2–3.4	2.0′
	YAN_st	Cube	25	25	30–250	8.3–3.1	2.0′
Macdonald et al. (1998)	MCDb_al	Cube	100	100	48–910	7.8–4.0	2.0′
	MCDb_st	Cube	100	100	48–910	6.3–3.6	2.0′
Poggi et al. (2004)	PGG_04	Plant	120	4	32.2–515	17.2–3.7	2.0′
Kang et al. (2019)	KAN_19	Plant	3.5–15.0	5.2–13.2	3.7–156	17.0–4.6	2.4
Li and Katul (2022)**	LI_22	Cube	–	–	80–438	6.7–1.5	2.0′
Placidi and Ganapathisubramani (2015)	PLA_15	Cube	7.8–15.6	11.4	120–240	5.5–1.4	2.0′

Table 2 Summary of published experimental and simulation results from literature (* field experiment, ** numerical simulation). Here the Data ID is the legend code used in Figs. 3, 4, 5, 6, 8. As before, the C_S is the fixed ground surface drag coefficient ($'$ is used when not provided by the authors), C_R and c_A are the free parameters obtained from nonlinear regression and R^2 is the coefficient of determination

Data ID	Rough Type	C_S	C_R	c_A	R^2
RTE	Plant	0.003	0.42	0.92	1.00
OL	Cube	0.003	0.30	0.01	0.98
GJR*	Plant	0.003	0.20	0.17	−4.91
WA_pla	Plant	0.0018	0.26	0.66	0.99
WA_cub	Cube	0.0019	0.33	0.54	0.97
MCD_al	Cube	0.002′	0.52	0.75	0.99
MCD_st	Cube	0.002′	0.93	0.88	0.92
WLF*	Plant	0.0052	0.26	0.72	0.75
LAN*	Plant	0.004	0.11	0.01	0.97
YAN_al**	Cube	0.002′	0.48	0.41	1.00
YAN_st**	Cube	0.002′	0.52	0.26	0.98
MCDb_al	Cube	0.002′	0.32	0.49	0.32
MCDb_st	Cube	0.002′	0.60	0.66	0.19
PGG_04	Plant	0.002′	0.09	0.01	0.93
KAN_19	Plant	0.0024	0.42	0.99	0.96
LI_22	Cube	0.002′	1.22	1.17	0.38
PLA_15	Cube	0.002′	1.57	1.56	0.091

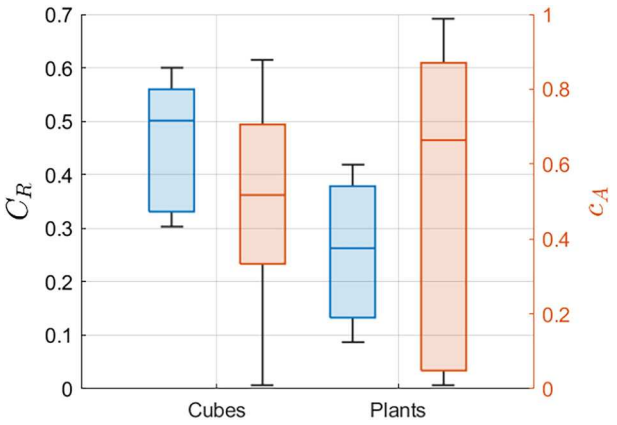

Fig. 2 Box plot of the optimized drag coefficient C_R (left ordinate, blue boxes) and scaling coefficient c_A (right ordinate, red boxes) obtained from the non linear regression for the two roughness shapes (cubes and plants) and all data sets

were 0.95, 0.91 and −0.04 for low, medium and high vegetation density, respectively. Lower R^2 values were also obtained for field experiments, which are typically characterized by large uncertainties and heterogeneous morphology not captured by λ alone (see GJR, WLF, MCDb_al and MCDb_st in Table 2).

As shown in Fig. 2, the variability in c_A exceeds that of C_R, with no significant differences observed between cubes and plants. The variability in C_R across experiments could be partly foreshadowed given that the dependence of C_R on the Reynolds number was not considered. However, because of the fitting procedure, this variability could also depend on

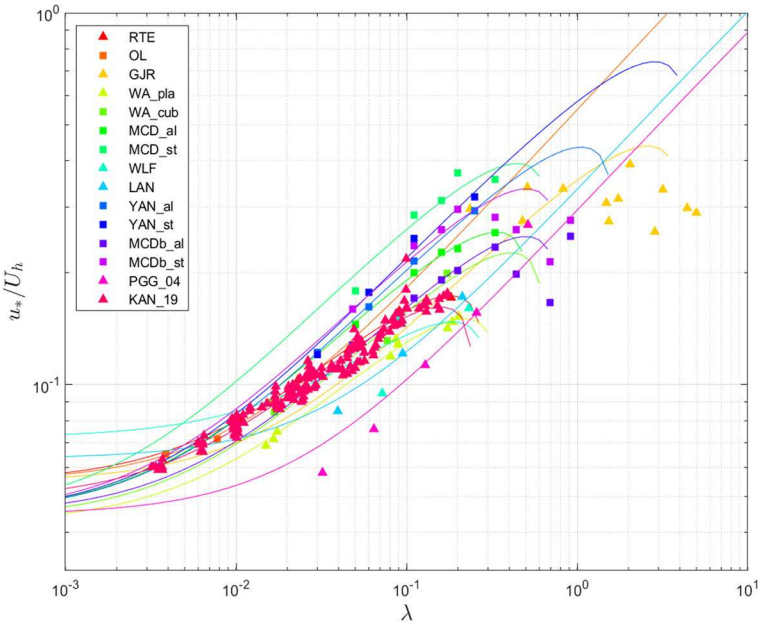

Fig. 3 The variation of u_*/U_h (ordinate) with frontal area index λ (abscissa) for plants (triangles) and cubes (squares). The R92 (i.e. Eq. 39) is shown in solid lines for the optimized parameters

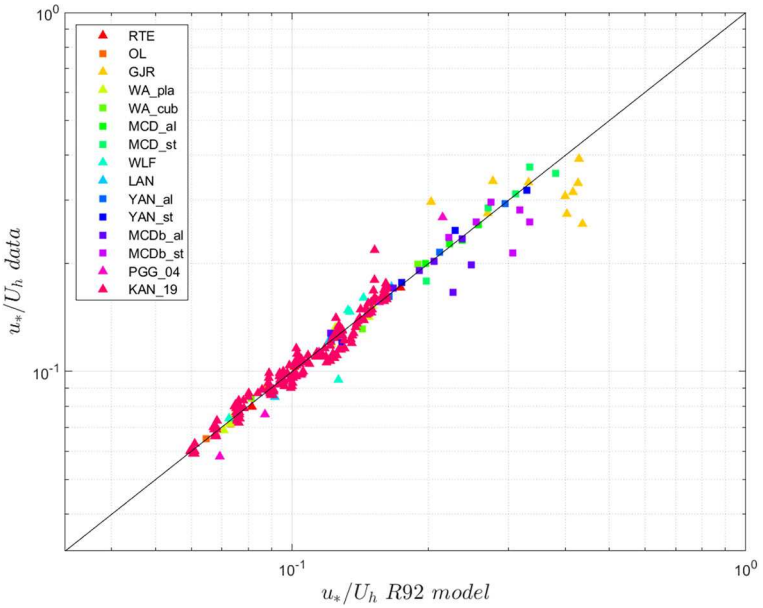

Fig. 4 Evaluation of R92 for predicting u_*/U_h. The experimental and numerical measurements of u_*/U_h (ordinate) are compared with predictions of u_*/U_h (abscissa) using the optimized parameters for plants (triangles) and cubes (squares)

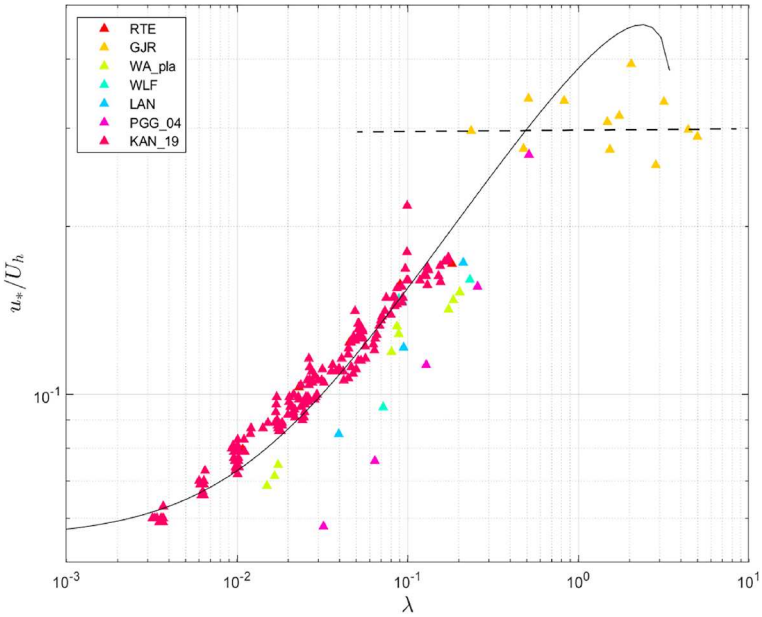

Fig. 5 The experimental results of u_*/U_h (ordinate) along with the frontal area index λ (abscissa) for plants compared with the mean parameterized Eq. 39 ($C_S = 0.002$, $C_R = 0.24$, $c_A = 0.19$)

other parameters not accounted for in the model. Despite a higher degree of heterogeneity in shapes, the range of C_R for plants is surprisingly similar to that of cubes. However, the parameter c_A exhibits a wider spread suggesting that the definitions of A and V in R92 might oversimplify quantities that are influenced by factors beyond those already incorporated in R92 (i.e. λ and γ), such as planar area index, aspect ratio, frontal solidity, internal porosity of rough elements, the roughness of the surface skin, or the dissipation rate of turbulent kinetic energy to name a few. To move R92 to an operational form, the data were also compared to predictions from Eq. 39 using values of $C_R = 0.24$ and $c_A = 0.19$ for plants and $C_R = 0.53$ and $c_A = 0.63$ for cubes, obtained by nonlinear regression of all data from each roughness element type, regardless of the data set. This comparison is shown in Fig. 5 for plants and Fig. 6 for cubes. Remarkably, despite being computed with approximate parameters, the R92 approach closely aligns with the experimental results. The R^2 for the data modeled with those C_R and c_A was 0.79 for cubes and 0.86 for vegetation, offering a pragmatic approach to large-scale models. The R92 has no solution for $\lambda > \lambda_c$ where λ_c is given by:

$$\lambda_c = \frac{C_R + \sqrt{C_R^2 + 4C_S(ec_A/2)^2}}{2(ec_A/2)^2}, \tag{45}$$

this theoretical upper bound is $\lambda_c = 3.6$ for plants and $\lambda_c = 0.7$ for cubes based on the suggested parameters. However, this parameterization establishes an upper bound for the R92 model, which appears to diminish in effectiveness for $\lambda \geq 0.3$, observed for both plants and cubes and in agreement with previous works (Katul et al. 2004).

To provide a benchmark to R92, another simplified drag partition model derived from first order closure arguments (Harman and Finnigan 2007) and hereafter referred to as HF7, is employed. According to HF7, when the canopy density is sufficiently large to ensure

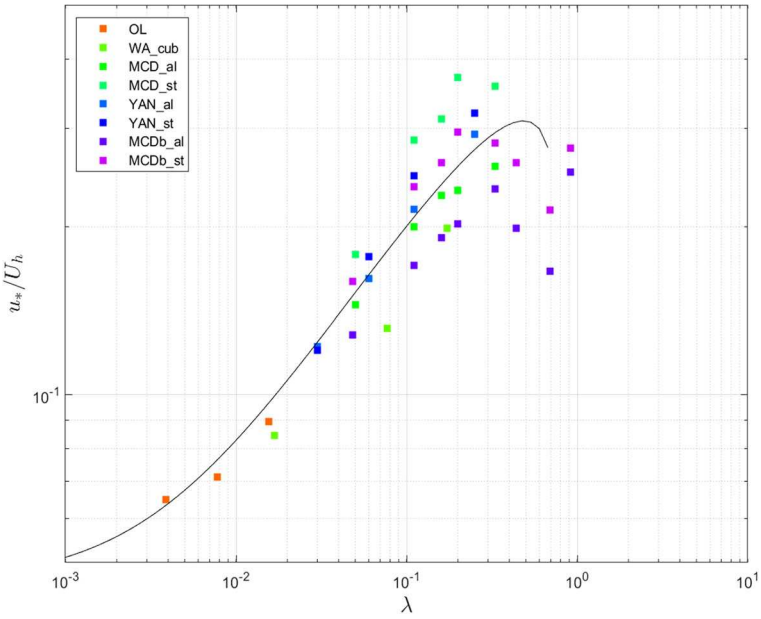

Fig. 6 The experimental and numerical results of u_*/U_h (ordinate) along with the frontal area index λ (abscissa) for cubes compared with the mean parameterized Eq. 39 ($C_S = 0.002$, $C_R = 0.53$, $c_A = 0.63$)

an inflection point in the velocity profile (usually at the canopy top), the resulting mixing length $L_m = 2L_c/\gamma^3$ may be assumed constant, where L_c is an adjustment length scale $L_c = (2C_R\gamma/h)^{-1}$. This argument, when combined with a first order closure for the mean momentum, leads to an exponential in-canopy mean velocity profile:

$$\frac{U(z)}{U_h} = \exp\left[-\frac{h}{\gamma L_m}\left(1 - \frac{z}{h}\right)\right], \tag{46}$$

where $z = 0$ is referenced to the ground. This first-order closure model assumes that $\tau = (K_m)dU/dz$, the eddy viscosity is $K_m = L_m|dU/dz|$ and it predicts $\tau = \tau_S \exp\left(2C_R\gamma^2\lambda\right)$. Using $\tau_S = \rho C_s U_h^2$, HF7 now predicts:

$$\frac{1}{\gamma^2} = C_S \exp\left(2C_R\lambda\gamma^2\right). \tag{47}$$

HF7 can also be compared with the data collected herein using the same methodology adopted for R92. The effectiveness of the model to predict u_*/U_h is shown in Fig. 7. HF7 appears to be slightly less effective than R92 in predicting γ for all the tested ranges of λ with an R^2 equal to 0.94, 0.85 and -1.49 for low, medium and high vegetation density respectively. This agreement between the experimental data and HF7 is a surprise given that the assumptions employed in HF7 should apply for dense canopies only. Indeed, for low values of λ the performance of HF7 is comparable to that of R92, and only for high λ R92 outperforms HF7.

Returning to the evaluation of R92, a comparison with two other studies for cuboids is conducted and shown separately in Fig. 8. These studies, which cover LES (Li and Katul 2022) and laboratory experiments with LEGO as obstacles (Placidi and Ganapathisubramani 2015) are separated from the other cube studies because they explore how u_*/U_h vary when the planar area density is altered for a preset λ. Also, $\lambda > 0.1$ in both studies, thus approaching

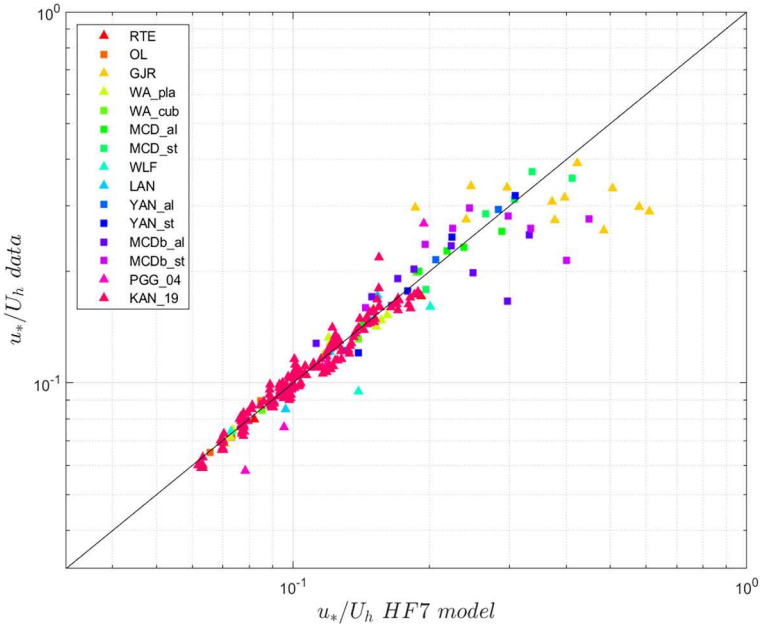

Fig. 7 Evaluation of HF7 for predicting u_*/U_h. The experimental and numerical measurements of u_*/U_h (ordinate) are compared with predictions of u_*/U_h (abscissa) using the optimized parameters for plants (triangles) and cubes (squares)

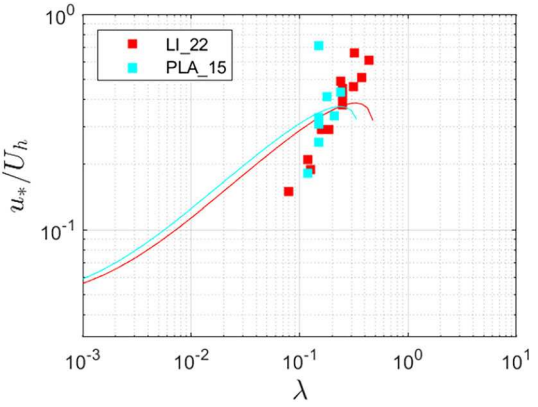

Fig. 8 Relation between u_*/U_h and λ for cuboid experiments and LES runs where the frontal area and the planar area both vary

the range where R92 acknowledged potential failure ($\lambda = 0.3$) due to wake interference with obstacle placement. While these two studies reasonably agree with each other, R92 fails to predict u_*/U_h from λ alone. This failure underscores the role of the planar area index (i.e. length and width are the defining obstacle geometry) in altering the shelter area beyond width and height (considered in the roughness area), which is neglected in R92. Nonetheless, the collapse of the two data sets with λ is simultaneously surprising and encouraging, and perhaps hints that R92 may be modified to include such effects. This modification is better left for a future study when more data sets will be available.

4 Conclusions

A drag partition model (R92) that separates the overall stress into contributions from roughness obstacles and from the ground was analyzed and evaluated with data and simulations collected over the past 3 decades. R92 was also compared to models that are based on first-order closure principles where the mixing length was presumed constant. By and large, R92 was shown to outperform such models when evaluated across a wide range of roughness densities. The work here focused on providing a stochastic framework for analyzing the effects of random obstacle additions for R92. Under some restrictive conditions, these revisions recover the re-normalized background stress proposed by R92 but in an ensemble-averaged sense. Such a stochastic averaging formalizes the up-scaling from individual to multiple roughness elements in R92 and identifies as well as clarifies some of the assumptions behind the stress re-normalization used in R92. An important condition for the validity of R92 is that the roughness elements are distributed homogeneously throughout the surface area and do not form clusters or isolated patches. Agreement between R92 and published data on cubes and vegetation-like roughness elements is acceptable for most data sets (many of which were collected after R92 was published). A poor performance was recorded for high roughness densities where wake interference between shelter areas is to be expected. This shortcoming was already addressed in R92 on intuitive grounds, while here it is formalized by the proposed stochastic approach. The mean value of $C_R = 0.24$ for plants is close to the value reported by R92 ($C_R = 0.3$). Using a single C_R and c_A for plants (C_R=0.24 and c_A=0.19) and cubes (C_R=0.53 and c_A=0.63) captures the u_*/U_h variations with frontal area density λ. For $\lambda \geq 0.3$, the modeled u_*/U_h degrades when using R92 without modification – though selecting a constant value of u_*/U_h=0.3 appears superior as already proposed by R92 and shown to be reasonable for many terrestrial vegetation studies (Katul et al. 2004). For high λ and for cases where the planar area density variations are large at a preset λ, the R92 performance leaves much to be desired and is worth exploring further. Despite this limitation, it may be surmised that the simplicity, the theoretical foundations, and the broad experimental support for R92 makes it practical to implement in large-scale weather forecasting and climate related models.

Acknowledgements EB acknowledges Politechnico di Torino (Italy) for supporting the visit to Duke University. GK acknowledges support from the U.S. National Science Foundation (NSF-AGS-2028633) and the U.S. Department of Energy (DE-SC0022072). DP acknowledges support from Fondo europeo di sviluppo regionale (FESR) for project Bacini Ecologicamente sostenibili e sicuri, concepiti per l'adattamento ai Cambiamenti ClimAtici (BECCA) in the context of Alpi Latine COoperazione TRAnsfrontaliera (ALCOTRA) and project Nord Ovest Digitale e Sostenibile - Digital innovation toward sustainable mountain (Nodes - 4). DV and CM acknowledge European Union's Horizon 2020 research and innovation programme under the Marie Sklodowska-Curie grant agreement No 101022685 (SHIEELD).

Funding Open access funding provided by Politecnico di Torino within the CRUI-CARE Agreement.

References

Aberle J, Järvelä J (2013) Flow resistance of emergent rigid and flexible floodplain vegetation. J Hydraul Res 51(1):33–45

Chappell A, Webb NP, Leys JF, Waters CM, Orgill S, Eyres MJ (2019) Minimising soil organic carbon erosion by wind is critical for land degradation neutrality. Environ Sci Policy 93:43–52

Coceal O, Belcher SE (2004) A canopy model of mean winds through urban areas. Q J R Meteorol Soc 130(599):1349–1372

Gardiner B (2021) Wind damage to forests and trees: a review with an emphasis on planted and managed forests. J For Res 26(4):248–266

Gardiner B, Peltola H, Kellomäki S (2000) Comparison of two models for predicting the critical wind speeds required to damage coniferous trees. Ecol Model 129(1):1–23

Giridharan R, Emmanuel R (2018) The impact of urban compactness, comfort strategies and energy consumption on tropical urban heat island intensity: A review. Sustain Cities Soc 40:677–687

Grimmond CSB, Oke TR (1999) Aerodynamic properties of urban areas derived from analysis of surface form. J Appl Meteorol Climatol 38(9):1262–1292

Harman IN, Finnigan JJ (2007) A simple unified theory for flow in the canopy and roughness sublayer. Boundary-Layer Meteorol 123:339–363

Hesp P (2002) Foredunes and blowouts: initiation, geomorphology and dynamics. Geomorphology 48(1–3):245–268

Huai Wx, Li S, Katul GG, My Liu, Yang Zh (2021) Flow dynamics and sediment transport in vegetated rivers: a review. J Hydrodyn 33(3):400–420

Ishugah T, Li Y, Wang R, Kiplagat J (2014) Advances in wind energy resource exploitation in urban environment: a review. Renew Sustain Energy Rev 37:613–626

Jamei E, Ossen D, Seyedmahmoudian M, Sandanayake M, Stojcevski A, Horan B (2020) Urban design parameters for heat mitigation in tropics. Renew Sustain Energy Rev 134(110):362

Kang L, Zhang J, Zou X, Cheng H, Zhang C, Yang Z (2019) Experimental investigation of the aerodynamic roughness length for flexible plants. Boundary-Layer Meteorol 172:397–416

Katul G, Grönholm T, Launiainen S, Vesala T (2011) The effects of the canopy medium on dry deposition velocities of aerosol particles in the canopy sub-layer above forested ecosystems. Atmos Environ 45(5):1203–1212

Katul GG, Mahrt L, Poggi D, Sanz C (2004) One-and two-equation models for canopy turbulence. Boundary-Layer Meteorol 113:81–109

Katul GG, Grönholm T, Launiainen S, Vesala T (2010) Predicting the dry deposition of aerosol-sized particles using layer-resolved canopy and pipe flow analogy models: Role of turbophoresis. J Geophys Res Atmos 115(D12)

Kok JF, Parteli EJ, Michaels TI, Karam DB (2012) The physics of wind-blown sand and dust. Rep Prog Phys 75(10):106,901

Lancaster N, Baas A (1998) Influence of vegetation cover on sand transport by wind: field studies at owens lake, california. Earth Surface Processes and Landforms. J British Geomorphol Group 23(1):69–82

Li Q, Katul G (2022) Bridging the urban canopy sublayer to aerodynamic parameters of the atmospheric surface layer. Boundary-Layer Meteorol 185(1):35–61

Macdonald R (2000) Modelling the mean velocity profile in the urban canopy layer. Boundary-Layer Meteorol 97:25–45

Macdonald R, Griffiths R, Hall D (1998) An improved method for the estimation of surface roughness of obstacle arrays. Atmos Environ 32(11):1857–1864

Marticorena B, Bergametti G (1995) Modeling the atmospheric dust cycle: 1. design of a soil-derived dust emission scheme. J Geophys Res Atmos 100(D8):16,415-16,430

Martilli A, Clappier A, Rotach MW (2002) An urban surface exchange parameterisation for mesoscale models. Boundary-Layer Meteorol 104:261–304

Nepf HM (1999) Drag, turbulence, and diffusion in flow through emergent vegetation. Water Resour Res 35(2):479–489

Nepf HM (2012) Hydrodynamics of vegetated channels. J Hydraul Res 50(3):262–279

Ng E, Yuan C, Chen L, Ren C, Fung JC (2011) Improving the wind environment in high-density cities by understanding urban morphology and surface roughness: A study in hong kong. Landsc Urban Plan 101(1):59–74

Okin G, Gillette D, Herrick J (2006) Multi-scale controls on and consequences of aeolian processes in landscape change in arid and semi-arid environments. J Arid Environ 65(2):253–275

Okin GS (2008) A new model of wind erosion in the presence of vegetation. J Geophys Res Earth Surf 113(F2)

Placidi M, Ganapathisubramani B (2015) Effects of frontal and plan solidities on aerodynamic parameters and the roughness sublayer in turbulent boundary layers. J Fluid Mech 782:541–566
Poggi D, Porporato A, Ridolfi L, Albertson J, Katul G (2004) The effect of vegetation density on canopy sub-layer turbulence. Boundary-Layer Meteorol 111:565–587
Raupach M (1992) Drag and drag partition on rough surfaces. Boundary-Layer Meteorol 60(4):375–395
Raupach M, Gillette D, Leys J (1993) The effect of roughness elements on wind erosion threshold. J Geophys Res Atmos 98(D2):3023–3029
Ravi S, Breshears DD, Huxman TE, D'Odorico P (2010) Land degradation in drylands: interactions among hydrologic-aeolian erosion and vegetation dynamics. Geomorphology 116(3–4):236–245
Ren C, Yang R, Cheng C, Xing P, Fang X, Zhang S, Wang H, Shi Y, Zhang X, Kwok YT et al (2018) Creating breathing cities by adopting urban ventilation assessment and wind corridor plan-the implementation in chinese cities. J Wind Eng Ind Aerodyn 182:170–188
Shao Y (2008) Physics and modelling of wind erosion. Springer
Shao Y, Dong C (2006) A review on East Asian dust storm climate, modelling and monitoring. Global Planet Change 52(1–4):1–22
Shao Y, Yang Y (2008) A theory for drag partition over rough surfaces. J Geophys Res Earth Surf 113(F2)
Tennekes H, Lumley JL (1972) A first course in turbulence. MIT press
Vargas-Luna A, Crosato A, Uijttewaal WS (2015) Effects of vegetation on flow and sediment transport: comparative analyses and validation of predicting models. Earth Surf Proc Land 40(2):157–176
Walter B, Gromke C, Lehning M (2012) Shear-stress partitioning in live plant canopies and modifications to raupach's model. Boundary-Layer Meteorol 144(2):217–241
Wolfe SA, Nickling W (1996) Shear stress partitioning in sparsely vegetated desert canopies. Earth Surf Proc Land 21(7):607–619
Yang XI, Sadique J, Mittal R, Meneveau C (2016) Exponential roughness layer and analytical model for turbulent boundary layer flow over rectangular-prism roughness elements. J Fluid Mech 789:127–165
Yu Y, Ginoux P (2022) Enhanced dust emission following large wildfires due to vegetation disturbance. Nat Geosci 15(11):878–884
Zender CS, Bian H, Newman D (2003) Mineral dust entrainment and deposition (dead) model: Description and 1990s dust climatology. J Geophys Res Atmos 108(D14)